Clays and Clay Minerals, Vol. 42, No. 2, 137–147, 1994.

Fe-SPECIATION IN KAOLINS: A DIFFUSE REFLECTANCE STUDY

NATHALIE MALENGREAU,[1,*] JEAN-PIERRE MULLER,[1,2] AND GEORGES CALAS[1]

[1] Laboratoire de Minéralogie-Cristallographie, URA CNRS 09
Universités de Paris 6 et 7, 4 Place Jussieu, 75 252 Paris Cedex 05, France

[2] O.R.S.T.O.M., Département T.O.A.
213 Rue La Fayette, 75 480 Paris Cedex 10, France

Abstract—Diffuse reflectance spectra of kaolins have been recorded in samples from different environments. They show the systematic presence of Fe-oxides, even in bleached kaolins, with no contribution from the Fe^{3+} ions substituted in kaolinite. Second derivative spectra of various Fe-phases (hematite, goethite, lepidocrocite, maghemite, akaganeite, ferrihydrite and Fe-polymer) may be differentiated by the position of a diagnostic band corresponding to the $2(^6A_1) \rightarrow 2(^4T_1(^4G))$ transition. The systematic comparison of diffuse reflectance spectra of unbleached and bleached kaolins has demonstrated the differences between the Fe-oxides occurring as coatings and as occluded phases. The features observed in second derivative spectral curves are consistent with assignments of crystal field transitions to goethite, hematite, akaganeite, and aged hydrous ferric oxides. The optical determination of the Fe-phases associated to kaolins assists in the interpretation of the formation conditions of these minerals.

Key Words—Diffuse reflectance spectroscopy, Fe-speciation, Kaolin, Second derivative spectra.

INTRODUCTION

Kaolins are among the most widespread materials at the Earth's surface. They occur under a wide range of geological conditions, including surficial weathering, sediment deposition, and low-temperature hydrothermal alteration (Murray, 1988). Besides minerals of the kaolinite group, natural kaolins commonly contain (Al, Fe)-oxides and oxyhydroxides and Ti-oxides, which chemical and physical treatments do not easily remove (Herbillon *et al.*, 1976; Jepson, 1988).

The forms of Fe associated with natural kaolinites can be used as an indicator of the conditions of formation and evolution of kaolins (Kampf and Schwertmann, 1983), and they participate in the control of the hydrogeochemical cycles of the elements at the Earth's surface (Davis and Kent, 1990). Furthermore, Fe compounds have undesirable effects on properties of industrial kaolins (Jepson, 1988). Whether ferric ions are substituted in the kaolinite structure or occur as separated phases is often uncertain (Muller and Calas, 1993). The low Fe-content of most deferrated kaolins and the finely divided nature of the associated Fe-containing phases limit the use of most methods (HRTEM, Mössbauer effect, EPR spectroscopy) to answer this question (Jepson and Rowse, 1975; Bonnin *et al.*, 1982; Angel and Vincent, 1978).

Diffuse reflectance spectroscopy has previously been used to investigate natural and synthetic Fe-oxides (Sherman *et al.*, 1982; Sherman and Waite, 1985; Morris *et al.*, 1985) and clays, including Fe-bearing soil kaolins (Karickhoff and Bailey, 1973; Kosmas *et al.*, 1984; Barron and Torrent, 1986). It has been used to monitor the influence of the modification of kaolin optical properties, e.g., scattering and brightness, as a function of the Fe-impurity content (Jepson, 1988). We present a determination of the Fe-oxides intimately associated with kaolinite, using second derivative diffuse reflectance spectroscopy. These Fe-oxides have optical spectral properties similar to those of goethite, hematite, akaganeite, or aged hydrous ferric oxides, depending on the formation conditions of kaolin.

MATERIALS

Natural kaolins

Highly ordered (KGa-1) and poorly ordered (KGa-2) sedimentary kaolins are used as reference materials from the late Cretaceous and early Tertiary Georgia deposits, respectively (Murray, 1988; van Olphen and Fripiat, 1979). Their degree of disorder is directly related to their total iron content (Table 1). Although X-ray diffraction (XRD) only barely detects the presence of accessory anatase, the Georgia kaolins contain various accessory minerals including quartz, micas, smectite, and heavy minerals such as magnetite, ilmenite, zircon, and goethite (Patterson and Murray, 1984; Jepson, 1988).

Well-ordered hydrothermal kaolins GB1 and GB3 come from a china clay deposit located within the Cornubian ore field of southwest England (St. Austell, Cornwall: Exley and Phil, 1959). Epithermal hydrothermal systems were involved in the development of these primary, granite-hosted kaolins (Jackson *et al.*, 1989). These samples contain only minor amounts of

* Present address: Department of Soil Science, University of California, Berkeley, CA 94720.

Copyright © 1994, The Clay Minerals Society

https://doi.org/10.1346/CCMN.1994.0420204 Published online by Cambridge University Press

Table 1. Analytical Fe contents of unbleached and bleached kaolins.

Samples	Fe_2O_3 (%)	
	Unbleached	Bleached
KGa-1	0.24	0.21
KGa-2	1.16	0.88
GB1	0.42	0.40
GB3	0.57	0.53
C15	0.60	0.83[1]
A6a	0.90	0.28
R1	12.41	1.20
R2	8.50	1.20

[1] Fraction > 2 micrometers.

Fe-impurities (Table 1). Several Fe-free phases were mentioned in the literature, such as muscovite, quartz, and feldspar (Jepson, 1988). Samples C15 and A6a are kaolins from hydrothermally altered ignimbritic tuffs of Tertiary age (Nopal I U-deposit, Chihuahua, Mexico: Calas, 1977; Aniel and Leroy, 1985). C15 sample is a white kaolin from a fissure system close to a U-mineralized breccia pipe, while A6a sample occurs as pseudomorphs of feldspars, also located in the breccia pipe (Muller *et al.*, 1990). Only kaolinite was detected by XRD in all these samples.

The soil kaolins were obtained from two lateritic weathering profiles. The first profile was developed on a gneissic basement under humid conditions and dense forest cover (East Cameroon). Typical profiles exhibit three main zones from bottom to top: a saprolite, a ferruginous nodular zone, and a clayey topsoil zone (Muller and Bocquier, 1986, 1987; Muller, 1988; Boudeulle and Muller, 1988). Sample R1 is a red, soft clay-iron oxide matrix that surrounds ferruginous nodules in the nodular zone. The second profile was formed from detrital materials under a dry tropical climate and savanna cover (Llanos area, East Colombia) and is composed of three zones from bottom to top: an indurated ferruginous plinthite; a red, soft, clayey zone; and an overlying yellow zone (Faivre *et al.*, 1983). Sample R2 is a red material from the red clayey zone. The associated Fe phases identified by XRD are goethite and hematite. These Fe-oxides account for the high Fe content of the soil kaolins (Table 1). R2 sample also contain some gibbsite. The goethite/goethite+hematite ratios are 45% and 65% in R1 and R2, respectively. The Al content in hematite and goethite from the R1 sample is 4 mole % and 15 mole %, respectively (Muller, 1988).

All kaolins were bleached using the dithionite-citrate-bicarbonate (DCB) method of Mehra and Jackson (1960). This deferration treatment was conducted at two different temperatures: the Fe-poor kaolins (<1.5 wt. % Fe_2O_3) were treated six times, at a temperature of 80°C, with reagents changed every half an hour; and the Fe-rich samples R1 and R2 (about 10 wt. % Fe_2O_3) were bleached at room temperature for 256 hr, while monitoring the mineralogical and chemical composition of the samples and extracted solutions (Jeanroy *et al.*, 1991). The efficiencies of both types of treatments are similar (E. Jeanroy, personal communication). In contrast with the other samples, KGa-1, GB1, and GB3 kaolins show no significant difference in Fe content before and after deferration treatment, but all bleached kaolins still contain Fe (Table 1).

Reference samples

The reference kaolinite used in this study is a synthetic hydrothermal sample (Petit and Decarreau, 1990) with only trace impurities (less than 100 ppm Fe^{3+} detected by EPR). Pure Fe-oxides, including Al-goethite, used for calibrating second derivative diffuse reflectance spectra, were obtained from several sources. Monodisperse synthetic goethite and hematite were synthesized from ferrihydrite by R. M. Cornell (Schwertmann and Cornell, 1991; Cornell *et al.*, 1991), and their purity was confirmed by XRD and Mössbauer spectroscopy at 298 K and 77 K (G. Morin, personal communication). An Al-substituted goethite (33 mole % Al) was synthesized by U. Schwertmann (Schwertmann and Murad, 1990). A tetragonal maghemite, prepared according to the procedure of Schwertmann and Cornell (1991), was provided by J. M. D. Coey. Lepidocrocite and akaganeite were synthesized by J. M. Combes according to the procedures of Schwertmann and Thalmann (1976) and Murphy *et al.* (1976), respectively. Two types of hydrous ferric oxides (HFO) were studied: a ferric polymer synthesized by J.-Y. Bottero from ferric chloride at a hydrolysis OH/Fe ratio of 2.8, according to the procedure of Combes *et al.* (1989); and a 5-line ferrihydrite from a natural spring of La Soufrière volcano in Guadeloupe, which contains 9.16% SiO_2.

METHODS

Diffuse reflectance spectroscopy

Diffuse reflectance spectra were obtained between 7000 and 45,000 cm^{-1} in a digital form and at room temperature with a CARY 2300 spectrophotometer fitted with a 10-cm-diameter integrating sphere coated with halon. Samples, 1–2 mm thick, were back-filled into aluminum frames without any packing to minimize preferential orientation and specular reflection. Optically treated silica slides covered the sample holders. Diffuse reflectance measurements were made relative to halon, the absolute reflectance of which is 99% or higher over the spectral range of 28,600–5600 cm^{-1} (Weidner and Hsia, 1981). Since the transitions are a function of photon energy, the spectra were converted to a wavenumber basis (cm^{-1}). The spectral resolution varied from 1 nm in the UV region to 2 nm in the NIR region. The wavelength accuracy of the spectrophotometer, checked by using emission line peaks from

https://doi.org/10.1346/CCMN.1994.0420204 Published online by Cambridge University Press

deuterium, was within ±0.1 nm in the UV and visible regions.

In order to avoid optical saturation effects (see below), the strongly absorbing reference Fe-oxides were diluted to 1.0 wt. % with synthetic Na_2CO_3, a compound which shows no significant absorption in the spectral range considered. As a result of this dilution, only the most intense absorption bands are observed in the diffuse reflectance spectra of all reference Fe-oxides. The low intensity of the absorption bands measured in weakly absorbing kaolins was enhanced by immersing samples in paraffin oil (refractive index 1.47). The presentation of diffuse reflectance spectra of kaolins as an apparent absorbance function, Log I_0/I (where I_0 and I are the intensity of the light reflected by the reference and the sample investigated, respectively), further enhances the intensity of the weakly absorbing bands.

Data reduction: Application of the Kubelka-Munk theory

Most surficial materials may be considered as mineral mixtures with an intermediate transparent-opaque behavior in the visible range (Strens and Wood, 1979). The Kubelka-Munk (KM) formalism has previously been used to model the absorption of the light scattered by tightly packed Fe-oxides (Barron and Torrent, 1986; Jepson, 1988). This formalism is well suited, because it takes into consideration light scattering as well as absorption processes (Wendlandt and Hecht, 1966). A remission function is defined as $f(R_\infty) = (1 - R_\infty)^2/2R_\infty = k/s$, in which R_∞ is the diffuse reflectance of the sample and k and s are the absorption and scattering coefficient, respectively (Morris *et al.*, 1982). The scattering coefficient, s, may differ between the samples as it depends on the particle size as well as on particle shape and packing. The absorption coefficient, k, cannot be deduced directly from R_∞, unless the effects of scattering can be constrained by some independent means (Bedidi and Cervelle, 1993). In the UV spectral range, Fe-oxides are strong light absorbers and the specular component of the light reflection cannot be neglected (Strens and Wood, 1979). The dilution of reference Fe-oxides with sodium carbonate avoids this problem. In the present study, the absorbance and remission functions of all kaolins were normalized by reference to the intensity of the OH overtone at 7160 cm^{-1} of KGa-1 kaolin. If s is considered as a monotone function, modifications of absorbance and remission functions should reflect absorption variations due to impurities along a constant optical path within the kaolin mineral particles.

Noise reduction of the experimental spectra was first performed by fitting each spectrum with a cubic spline function, which is more amenable to numerical differentiation than the least-squares methods (Dunfield and Read, 1972). Second derivative functions were then calculated using a numerical method (Kosmas *et al.*, 1984; Huguenin and Jones, 1986). A key feature of the second derivative is its ability to show the location of ill-defined absorption bands and to resolve bands that are too close to be resolved in experimental spectra (Cahill, 1979). The position of the absorption bands is indicated by minima on the second derivative curves (Huguenin and Jones, 1986). The halfwidth of each band has been estimated from the separation between the minimum and the maximum measured in the second derivative. Because the absorption bands in Fe-oxide spectra are superimposed on a rising slope, their apparent position is shifted toward higher wavenumbers. Spectral simulations on diluted samples were also produced by fitting each spectrum with Gaussian absorption bands superimposed onto a Gaussian wing continuum. A similar accuracy was obtained on band positions by Gaussian decomposition, but the second derivative was preferred as it is easier to use. The actual band positions can be determined, from second derivative spectra, to within ±80 cm^{-1}.

RESULTS AND DISCUSSION

Reference Fe-phases

Diffuse reflectance spectra of Fe-oxides exhibit several absorption bands in the UV-visible range (Figure 1), which correspond to Fe^{3+}-crystal field transitions (Sherman and Waite, 1985). Opaque minerals, such as magnetite or ilmenite, have a low optical band gap and uniformly absorb radiation in the UV-visible region (Hunt *et al.*, 1971), resulting only in an increase in the overall remission function by a constant amount. Second derivative spectra show that the number and position of the absorption bands vary among the Fe-oxides (Figure 2). The most prominent transitions that occur in the visible-UV range are: 1) a weak absorption band near 15,000 cm^{-1} corresponding to the $(^6A_1) \rightarrow (^4T_2(^4G))$ transition; 2) a marked band located near 19,000–20,000 cm^{-1} corresponding to the $2(^6A_1) \rightarrow 2(^4T_1(^4G))$ transition; and 3) a band near 23,400 cm^{-1}, observed only for goethite, corresponding to the $(^6A_1) \rightarrow (^4E,^4A_1(^4G))$ transition. Slight differences are observed with the values given in the literature (Table 2), but the spectra reported earlier seem to be similar to those of reference samples investigated in this paper. It is indeed difficult to estimate the position of an absorption band from the experimental spectrum of pure Fe-oxides because the overall absorption slope strongly shifts the apparent position of these bands.

As the $2(^6A_1) \rightarrow 2(^4T_1(^4G))$ transition is observed at a different position in the various Fe-oxide references, we have used it as a diagnostic absorption band for the determination of Fe-oxides (Table 2). The $(^6A_1) \rightarrow (^4E,^4A_1(^4G))$ transition band was additionally used to distinguish the goethite with respect to lepidocrocite. The two diagnostic bands are shifted towards higher

https://doi.org/10.1346/CCMN.1994.0420204 Published online by Cambridge University Press

Table 2. Second derivative minimum positions and halfwidths of the main diagnostic band corresponding to the $2(^6A_1) \rightarrow 2(^4T_1(^4G))$ transition 1) for reference Fe-oxides and oxyhydroxides, ferrihydrite, and Fe-polymer determined in this work compared with the experimental band positions given in the literature; and 2) for the natural unbleached and bleached kaolins. The mineralogical interpretation of absorption bands observed in the kaolin spectra is also given.

	This work		Literature	
Reference Fe-phases	Position (cm^{-1})	Halfwidth (cm^{-1})	Position (cm^{-1})	Authors
Hematite	18,450	1590	18,900	Sherman and Waite (1985)
Goethite	20,330	2110	20,200	Kosmas *et al.* (1986)
Lepidocrocite	20,450	2810	20,620	Sherman and Waite (1985)
Akaganeite	19,920	1840	[2]	Sherman *et al.* (1982)
Maghemite	20,200	[1]	19,010	Sherman and Waite (1985)
	19,530	[1]		
Ferrihydrite	19,840	2480	[2]	Sherman *et al.* (1982)
Fe-polymer	19,570	3280	[2]	Evans and Adams (1980)
Unbleached kaolins	Position (cm^{-1})	Halfwidth (cm^{-1})		Mineralogical interpretation
KGa-1	19,960	1110	akaganeite/ferrihydrite	
KGa-2	20,370	2120	goethite	
GB1	20,160	1600	goethite	
GB3	20,160	1420	goethite	
C15	20,490	2770	goethite	
A6a	18,280	1440	hematite	
	20,370	1270	goethite	
R1	18,620	1455	Al-hematite	
	20,600	1620	Al-goethite	
R2	18,480	1560	hematite	
	20,325	1970	goethite	
Bleached kaolins	Position (cm^{-1})	Halfwidth (cm^{-1})		Mineralogical interpretation
KGa-1	19,960	1050	akaganeite/ferrihydrite	
KGa-2	20,010	1120	akaganeite/ferrihydrite	
GB1	20,200	1490	goethite	
GB3	20,200	1490	goethite	
C15	20,410	2320	goethite	
A6a	18,420	1110	(hematite)	
	20,490	1390	goethite	
R1	20,000	1480	akaganeite/ferrihydrite	
	20,660	1460	Al-goethite	
R2	18,520	1050	(hematite)	
	20,750	1310	Al-goethite	

[1] Undetermined, doublet of superimposed bands.
[2] Undetermined band position in the published spectrum.
(Hematite): phase present in very small amount.

wavenumbers when goethite is Al-substituted (Figure 2). The position of the $2(^6A_1) \rightarrow 2(^4T_1(^4G))$ transition band ranges from about 20,300 cm^{-1} for unsubstituted goethite to about 21,400 cm^{-1} for a substitution of 33 mole % Al, which is in good agreement with the findings of Kosmas *et al.* (1986). The only noticeable exception is the possible confusion between ferrihydrite and akaganeite because they show diffuse reflectance spectra with similar electronic transition energies. The closely related local structures of both compounds, recently shown by EXAFS (Combes *et al.*, 1989), explain the similarity of the Fe^{3+}-crystal field in these compounds. Another feature may assist in deciphering among the possible Fe-oxides; the halfwidth of the ferrihydrite absorption band is 1.3 times larger than that of akaganeite. In hematite, the intensity of the diagnostic band is enhanced by magnetic coupling between Fe^{3+} cations in face-sharing FeO_6 octahedra (Sherman and Waite, 1985). It is split in maghemite, in relation to the presence of Fe^{3+} in two distinct sites. Eventually, the diagnostic band of the Fe-polymer is broadened respective to the other phases, which reflects a distribution of the Fe^{3+}-environments in the disordered structure of this compound.

Natural kaolins

The reference kaolinite presents sharp peaks near 7000 cm^{-1}, which correspond to OH overtones, while it is featureless in the UV-visible range. The rising slope indicates light scattering by small particles (Figure 3). Natural kaolins differ from synthetic kaolinite in that they exhibit distinct absorption bands superimposed on the rising background in the UV-visible range. The positions and intensities of these bands vary among

https://doi.org/10.1346/CCMN.1994.0420204 Published online by Cambridge University Press

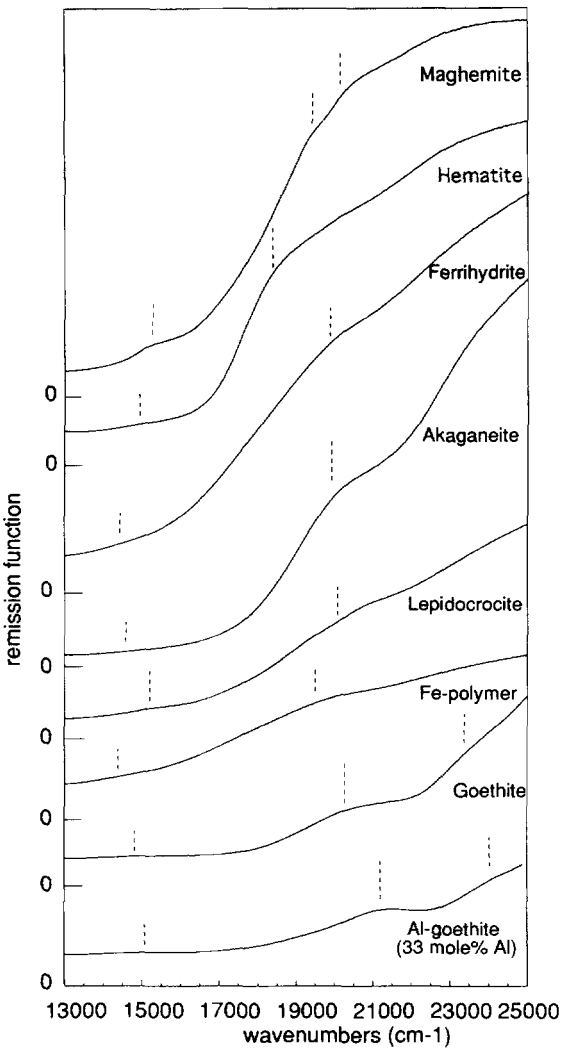


Figure 1. Raw spectra of diluted reference Fe oxides and oxyhydroxides, in the 13,000–25,000 cm^{-1} range. The vertical bars indicate absorption band positions; their length varies as a function of the apparent intensity of the band.

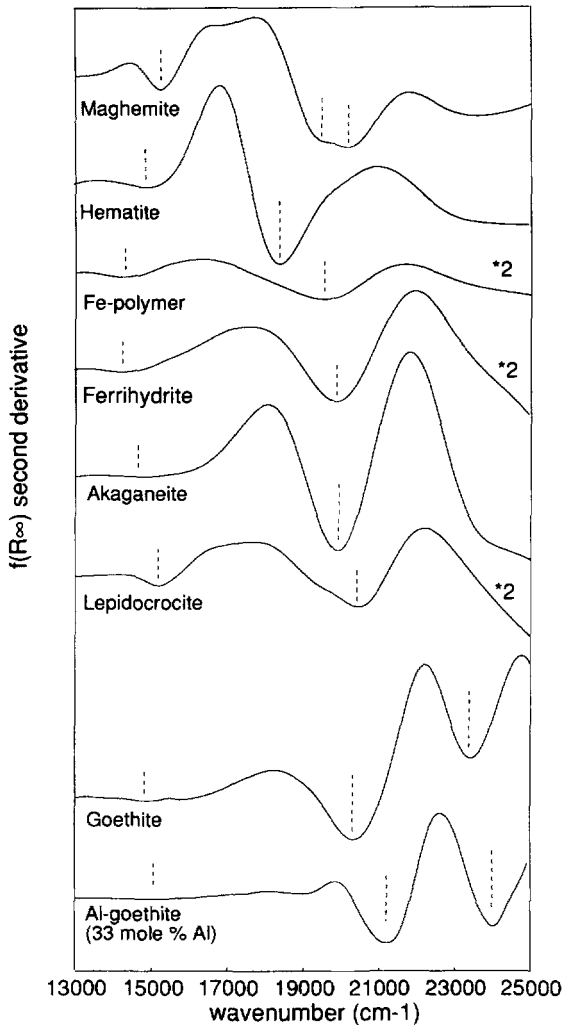


Figure 2. Second derivative curves of diluted reference Fe oxides and oxyhydroxides in the 13,000–25,000 cm^{-1} range. The absorption bands are indicated by dashed vertical bars, the length varying as a function of the apparent intensity of the band. The remission function values for Fe-polymer, ferrihydrite, and lepidocrocite spectra were increased twofold.

the samples. It should be noted that there is no evidence of crystal-field (CF) transitions due to isolated Fe^{3+}, Fe^{2+}, and Ti^{4+} cations within the kaolinite structure despite the presence of paramagnetic Fe^{3+} detected by EPR spectroscopy (Muller and Calas, 1993). Even for the field-independent CF transition near 22,500 cm^{-1} (Burns, 1985; Calas, 1986), the low values of the absorption coefficient k of spin-forbidden Fe^{3+} transitions prevent their observation in diffuse reflectance spectra. Similarly, no features corresponding to substituted octahedral Fe^{2+} are observed in the 9000–11,000 cm^{-1} range, although this cation was suspected to occur as an impurity in some kaolins (Angel and Vincent, 1978). Ti^{4+} atoms, which also may substitute for Al within the structure of natural kaolinites (Rengasamy, 1976), do not produce any CF transitions because of their $3d^0$ configuration. Most kaolins exhibit strong absorption bands near 30,000 cm^{-1}, evidently due to Ti–O charge transfer in ancillary TiO_2 phases such as anatase or Ti-oxide gels (Tossell *et al.*, 1974). Finally, an intense, broad band near 40,000 cm^{-1}, already reported in previous studies and attributed to an $O–Fe^{3+}$ charge transfer (Karickhoff and Bailey, 1973), was observed for some samples, perhaps related to the presence of Fe^{3+} substituted in the kaolinite structure. The other broad bands in the visible region are similar to those observed for the reference Fe-oxides, and the position of the diagnostic band due to the $2(^6A_1) \rightarrow 2(^4T_1(^4G))$ transition may be used to determine the Fe-oxides associated to kaolins (Table 2).

The diffuse reflectance spectra of the deeply colored

https://doi.org/10.1346/CCMN.1994.0420204 Published online by Cambridge University Press

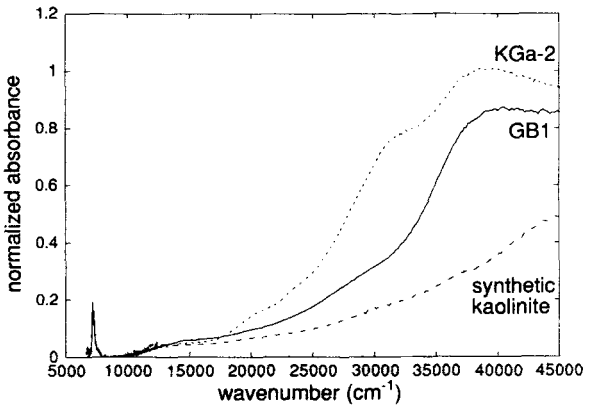


Figure 3. Diffuse reflectance spectra of a sedimentary (KGa-2), a hydrothermal (GB1), and an Fe-free synthetic kaolinite in the UV-visible-NIR range, normalized to OH feature.

soil kaolins R1 and R2 show two well-separated, intense absorption bands near 18,500 and 20,400 cm^{-1}, that confirm the presence of hematite and goethite, already detected by XRD (see above). In the R1 sample, the diagnostic band is shifted to higher wavenumbers by 170 and 270 cm^{-1}, relative to reference hematite and goethite, respectively. This shift indicates

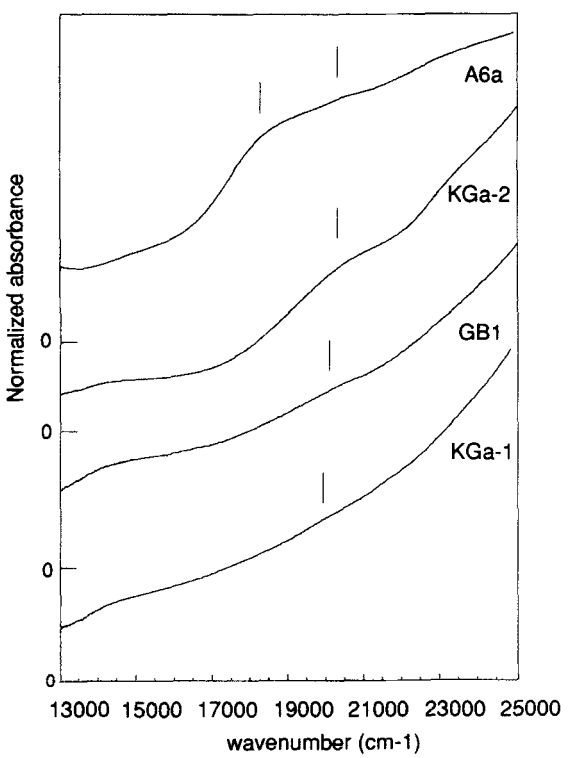


Figure 4. Raw spectra of unbleached hydrothermal (A6a, GB1) and sedimentary kaolins (KGa-1, KGa-2) in the visible range. The vertical bars indicate the positions of diagnostic bands determined from second derivative curves.

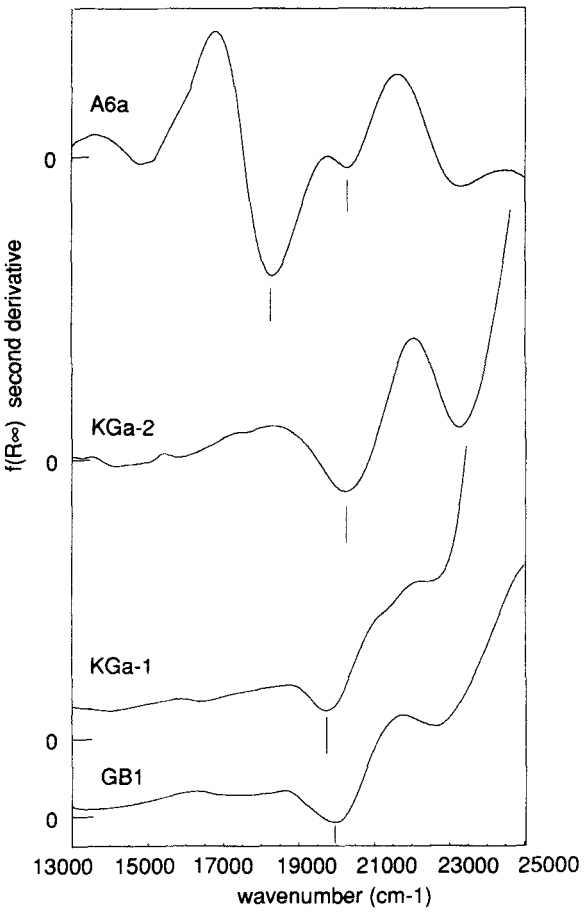


Figure 5. Second derivative curves of unbleached hydrothermal (A6a, GB1) and sedimentary kaolins (KGa-1, KGa-2) in the visible range. The vertical bars indicate the positions of diagnostic bands.

the presence of Al-bearing hematite and goethite, according to the spectral data on Al-goethite (see above) and Al-hematite (Kosmas *et al.*, 1986).

The diffuse reflectance and second derivative spectra of hydrothermal kaolins (Figures 4 and 5) exhibit the two absorption bands characteristic of goethite, although the position of the diagnostic band in the 20,150–20,500 cm^{-1} range shows some variations. Angel and Vincent (1978), using EPR spectroscopy, reported that the Cornish kaolin samples (GB1 and GB3) contained lepidocrocite. No lepidocrocite was identified in the present study. This discrepancy may arise from similar properties of superparamagnetic Fe-oxyhydroxide particles that do not enable an accurate determination of these Fe-oxides using EPR spectroscopy unless the shape and size are well constrained. The A6a kaolin displays an additional band near 18,300 cm^{-1}, which can be assigned to hematite.

The two sedimentary kaolins (Figures 4 and 5) present different signatures. The KGa-2 spectrum exhibits

https://doi.org/10.1346/CCMN.1994.0420204 Published online by Cambridge University Press

the two diagnostic bands of goethite near 20,370 and 23,400 cm^{-1}. In contrast, the KGa-1 spectrum presents an absorption band at 19,960 cm^{-1} that can be attributed to akaganeite or ferrihydrite. These results are also in disagreement with the findings of Angel and Vincent (1978), who concluded that these Georgia kaolins contained hematite. Here also, EPR spectroscopy barely deciphers among the superparamagnetic Fe-oxides particles.

Bleached kaolins

Optical spectra of bleached kaolins reveal a systematic presence of residual Fe-oxides and/or oxyhydroxides (Table 2).

The R1 sample displays three bands at 20,000 cm^{-1}, 20,660 cm^{-1}, and near 23,200 cm^{-1} (Figures 6A and 6B), with the disappearance of the band near 18,500 cm^{-1} ascribed to hematite. The band at 20,000 cm^{-1} can be attributed to akaganeite or ferrihydrite, although its halfwidth is closer to that of akaganeite (Table 2). The bands at 20,660 cm^{-1} and 23,200 cm^{-1} indicate the presence of Al-goethite. The band position at the end of the deferration treatment indicates a substitution of 12 mole % Al (Kosmas *et al.*, 1986), which is close to the amount of Al-substitution estimated from the XRD data (15 mole %) (Muller, 1988). The spectrum of the R2 sample also shows the two characteristic bands of an Al-goethite estimated to be about 14 mole % Al. In contrast to sample R1, a weak band near 18,520 cm^{-1}, only detected by sample immersion in paraffin oil, indicates the presence of small amounts of hematite. The absorbance values and the absorption band intensities are higher for bleached R2 than for bleached R1 although the total Fe content is identical in both samples (1.2 wt. % Fe_2O_3). EPR spectra show that superparamagnetic Fe-oxides have a smaller size in R1 as compared with R2 (Malengreau and Allard, unpublished data). A small particle size may account for a weaker light absorption in R1 diffuse reflectance spectrum, according to studies on simulated reflectance spectra of Fe-oxide powders (Bedidi and Cervelle, 1993).

The spectra of the four bleached hydrothermal kaolins exhibit the two bands characteristic of goethite (Table 2) and, unlike the bleached soil kaolins, no shift of the bands associated with the $2(^6A_1) \rightarrow 2(^4T_1(^4G))$ transition was observed. According to the intensity of the absorption bands, the goethite content is not affected by the deferration treatment while hematite is nearly removed in A6a.

The bleached sedimentary kaolins exhibit peculiar optical spectra with three bands that do not correspond to goethite or hematite. Two bands near 21,500 cm^{-1} and 23,000 cm^{-1} indicate the presence of Fe-bearing anatase. The third band, at 19,960 cm^{-1} and 20,010 cm^{-1} in KGa-1 and KGa-2, respectively, is characteristic of akaganeite or ferrihydrite (Figures 7A and 7B).

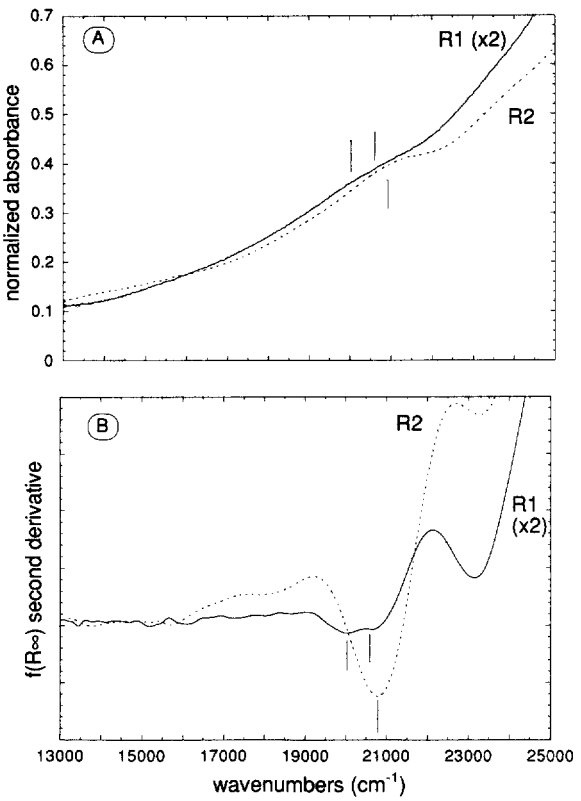


Figure 6. Raw spectra (A) and second derivative curves (B) of bleached soil samples (R1, R2) in the visible range. Remission function values for R1 have been multiplied by two for a better comparison of features with R2 sample. The band near 23,400 cm^{-1} is characteristic of goethite. The vertical bars on (A) indicate the positions of diagnostic bands determined from second derivative curves.

However, the halfwidths of these bands are smaller than those of reference samples (1100 cm^{-1} instead of 2000–3000 cm^{-1}: Table 2). This difference will be discussed below.

It is interesting to compare the speciation of Fe in bleached kaolinites having similar total Fe-contents, such as the hydrothermal C15 and the sedimentary KGa-2 kaolinite samples that both contain 0.8 wt. % Fe_2O_3 (Table 1). Sample C15 is characterized by a well-resolved, intense optical signal due to a goethite-like phase, as well as a low content of Fe^{3+} ions substituted in kaolinite and detected by EPR (Muller *et al.*, 1990). In contrast, sample KGa-2 lacks clear evidence of goethite according to optical spectra and presents an Fe^{3+} EPR signal three to four times more intense than sample C15 (Muller and Calas, 1993). These differences indicate that the Fe is mainly in the form of occluded Fe-oxides in C15, while it is mainly substituted within the kaolinite structure in KGa-2. In addition, C15 shows a weak EPR signal due to superparamagnetic Fe-oxides, as is typical of the hydrothermal kaolinites from this area (Muller *et al.*, 1990). This indicates that the

https://doi.org/10.1346/CCMN.1994.0420204 Published online by Cambridge University Press

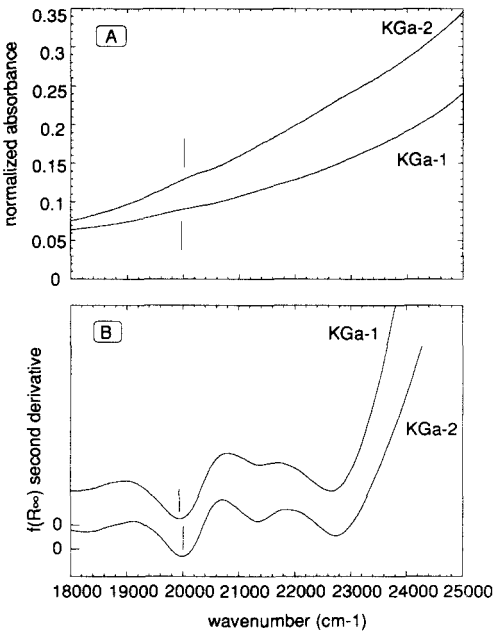


Figure 7. Raw spectra (A) and second derivative curves (B) in the absorption region (18,000–25,000 cm^{-1}) of bleached sedimentary kaolins (KGa-1, KGa-2) immersed in paraffin oil. The two bands near 21,000 cm^{-1} and 23,000 cm^{-1} are likely due to Fe-bearing anatase. The vertical bars on (A) indicate the positions of diagnostic bands determined from second derivative curves.

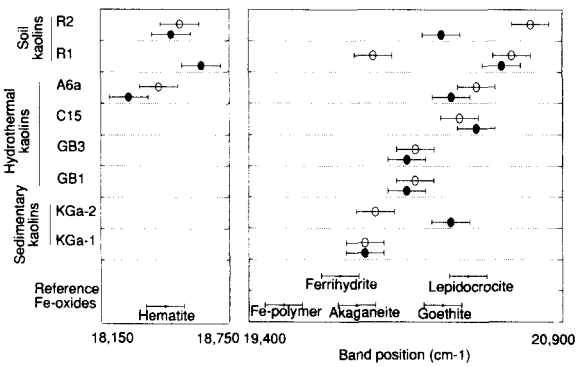


Figure 8. Summary of Fe-phases detected through DRS in the unbleached (●) and in the bleached kaolins (○) from this study. The position of the bands on second derivative curves can be compared with that of the characteristic bands of reference oxides. Error bars are within a ±80 cm^{-1} range.

goethite-like phases have a particle size greater than 10 nm. In contrast, the EPR signal of superparamagnetic Fe-oxides is more intense in KGa-2. This is consistent with the identification of akaganeite/ferrihydrite-like phases whose dimensions are probably too small (less than 10 nm) to enhance their superparamagnetic character.

DISCUSSION

The present study shows the differences between the Fe-oxide coatings and occluded phases in natural kaolins. As Fe-oxide coatings are more recent than the kaolinite crystals they surround and as they are easily bleached, they are thus sensitive to environmental changes after kaolin formation. In contrast, occluded Fe-oxides are contemporaneous (or may be syngenetic) with kaolinite and are protected from changing environmental factors according to their insensitivity to a deferration treatment. Thus, comparison between optical spectra of raw and bleached kaolins could be useful in deriving information on the conditions of kaolin formation and subsequent evolution (Table 2 and Figure 8).

The origin of the primary granite-hosted kaolinite deposits from Cornwall has been widely disputed for a number of years (Jackson *et al.*, 1989). Hypotheses were discussed in the literature on the possible hypogene or supergene origin of these kaolinites. On one hand, Alderton and Rankin (1983) provided evidence, from fluid inclusion studies of veins and altered granite materials, for both hypothermal (200°–500°C) and epithermal (less than 200°C) hydrothermal origin. On the other hand, Sheppard (1977) from stable isotope studies, and Bristow and Exley (in Jackson *et al.*, 1989) from observations of sections and cores gave evidence for a supergene origin by deep tropical weathering. In this present study, the optical evidence of goethite in GB1 and GB3 kaolins shows that kaolinite formation occurred at temperatures lower than 200°C, as goethite dehydrates into hematite at temperatures between 120° and 200°C (Watari *et al.*, 1983). In consideration of the hydrothermal characteristics of the EPR spectra of GB1 and GB3 samples (Muller and Calas, 1993), iron oxyhydroxides included within kaolinite particles can be considered as indicators of a temperature of less than 200°C (i.e., epithermal conditions). In the multistage model proposed by Bristow (1993), the GB1 and GB3 kaolins could have formed during the low-temperature water-rock interaction that would have followed an early hydrothermal activity.

The origin of kaolinite in the Nopal I hydrothermal alteration system is also under debate. Fluid inclusion studies (Leroy *et al.*, 1987) provide evidence for kaolinization at temperatures as high as 150°C, but stable isotope geochemistry indicates a hydrothermal origin at a lower temperature of about 60°C (Ildefonse *et al.*, 1990). The presence of the goethite-like phase in bleached C15 supports the lower (60°C) formation temperature, with the kaolinization process occurring in a shallow convective groundwater system. The presence of hematite coatings on particles of A6a kaolin provides evidence for a later higher temperature episode within the breccia pipe.

The evidence in soil kaolins of occluded particles with optical properties similar to Al-goethite is con-

https://doi.org/10.1346/CCMN.1994.0420204 Published online by Cambridge University Press

sistent with the idea that kaolinite and associated Al-goethite are syngenetic, the Fe content of kaolinite being correlated with the Al content of goethite (Muller, 1988). This syngenetic relationship is also supported by the epitaxial growth of goethite upon kaolinite evidenced in materials from lateritic soils (Boudeulle and Muller, 1988), where Fe-oxide clusters may have acted as nuclei for an epitaxial growth of goethitic phases. The determination of goethite and hematite from optical spectroscopy in unbleached R1 and R2 is consistent with XRD results (Muller and Bocquier, 1987). Hematite is completely removed after the deferration treatment of R1, but a small amount remains in R2. The observation that hematite, which constitutes about 65% of Fe-oxides in the unbleached sample, is dissolved during DCB treatment implies that its formation is after that of kaolinite, which confirms previous conclusions based on microscopic observations (Muller, 1988). The intimate association of a small amount of hematite and goethite within the R2 kaolinite could signify that they crystallized simultaneously with kaolinite. Owing to the control of the macroclimate on Fe-oxide formation (Schwertmann *et al.*, 1982), the presence of hematite in R2 would imply both higher temperatures and less rainfall than during the formation of R1. The presence of a ferrihydrite-like phase occluded within the bleached R1 sample is not readily explained. A possible explanation is that rapid crystallization of kaolinite allowed insufficient time for Fe-oxide formation from hydrous ferric oxides. A simultaneous inhibitory effect of growth poisons such as organic compounds could also be considered (Cornell and Schwertmann, 1979; Schwertmann, 1988).

Studies of thorium geochemistry (Dombrowski and Murray, 1984) support the idea that Georgia kaolins were originally formed from crystalline rocks under intense weathering conditions and then transported and deposited in adjacent coastal basin. However, EPR spectra show that sedimentary kaolins suffered diagenetic alteration (Muller and Calas, 1993). Diffuse reflectance spectra of bleached sedimentary and R1 soil kaolins both show the presence of an akaganeite/ferrihydrite-like phase, with similar band positions but different halfwidths (Table 2). Spectroscopic data would thus be consistent with sedimentary kaolins resulting from a limited modification of detrital soil kaolins during diagenesis.

The band positions of the diagnostic band of Fe-oxides in kaolins are similar to those observed in reference samples. However, with the exception of KGa-2 and C15 kaolins, it should be noted that the halfwidths measured in kaolins are narrower than in Fe-oxide references. The better defined features on the diffuse reflectance spectra may indicate an intimate association of these ferric phases with kaolinite, e.g., as surface precipitates on kaolinite (O'Day *et al.*, 1990). A relationship between properties of occluded Fe-oxides and the defect structure of kaolinite, as described by Plançon *et al.* (1988, 1989), could be expected if Fe-phases are sandwiched between the basal faces of kaolinite crystals. For instance, the concentration of Fe^{3+} substituted in distorted sites at the boundary of kaolinite coherent domains (Fe(I) sites: Muller and Calas, 1993), is correlated with the structural order (Meads and Malden, 1975; Mestdagh *et al.*, 1980). Fe clusters may act as nuclei for the epitaxial growth of Fe-phases. This intimate association between kaolinite and Fe-oxides could favor a better ordered Fe-oxide and then explain the narrower band halfwidths. HRTEM studies are in progress to confirm this hypothesis.

CONCLUSIONS

Diffuse reflectance spectroscopy method is a powerful tool for studying the Fe-speciation and the nature of iron oxides and oxyhydroxides in natural kaolins. Several conclusions can be derived from this study:

1) There is no evidence for Fe^{3+} or Fe^{2+} cations substituted in kaolinite, but Fe-oxides are ubiquitous. Diffuse reflectance spectroscopy may detect these Fe-oxides in kaolins, even as minor components which cannot be observed with other methods.
2) The use of second derivative spectra improves the resolution of diffuse reflectance data. Crystal field transitions do not occur at the same position in the various Fe-oxides, including Fe-polymers. The $2(^6A_1) \rightarrow 2(^4T_1(^4G))$ transition has been used as a diagnostic band for deciphering among the various Fe-oxides, including the Al-substitution rate in goethite and hematite.
3) Comparison of spectra of kaolins before and after a deferration treatment enables the identification of Fe-oxides in the form of coatings and of occluded phases. The distribution of Fe-oxides in kaolins was eventually used to provide a genetic interpretation. The significance of both types of Fe-oxides is different, as a) occluded Fe-oxides are indicators of the growth conditions of kaolinite and b) the coatings show the environmental changes subsequent to kaolinite formation.

The information drawn from diffuse reflectance spectroscopy of kaolins is illustrated by examples in the three main environments in which kaolins are found. In hydrothermal systems, the Fe-oxides indicate epithermal conditions ($T < 200°C$) during kaolinite formation, involving shallow convective groundwater systems, rather than high-temperature episodes of alteration as indicated by isotopes or fluid inclusions. Fe-oxides chronology is clarified in soil kaolins, in which the Fe-substituted kaolinite and Al-substituted goethite are syngenetic in soft, red materials from two tropical soils, with subsequent formation of hematite (the dominant soil Fe-oxide). The presence of akaganeite/ferrihydrite-like phases in the Cretaceous and

https://doi.org/10.1346/CCMN.1994.0420204 Published online by Cambridge University Press

Tertiary sedimentary kaolins support the hypothesis that sedimentary kaolinites derived from pre-existing deep weathering in a nearby emerged continent and were subsequently affected by basin diagenesis.

ACKNOWLEDGMENTS

The authors are much obliged to J.-Y. Bottero, J. M. D. Coey, R. M. Cornell, A. Decarreau, P. Ildefonse, A. Manceau, and U. Schwertmann for providing the reference samples used in the spectral calibrations, E. Jeanroy for deferrification of soil kaolinitic samples and A. Bedidi for fruitful discussions. Thanks are also due to M.-C. Sichère and H. Vachey for their assistance for the XRD determination and the chemical analyses, respectively. We also wish to thank J. K. Crowley and one anonymous reviewer for their valuable comments on the manuscript and C. C. Harvey for improving the English. This work was supported by the PEGI (CNRS-INSU-ORSTOM) program.

REFERENCES

Alderton, D. H. M. and Rankin, A. H. (1983) The character and evolution of hydrothermal fluids associated with the kaolinized St. Austell granite, SW England: *Geol. Soc. London. J.* **140,** 297–310.

Angel, B. R. and Vincent, W. E. J. (1978) Electron spin resonance studies of iron oxides associated with the surface of kaolins: *Clays & Clay Minerals* **26,** 263–272.

Aniel, B. and Leroy, J. (1985) The reduced uraniferous mineralizations associated with the volcanic rocks of the Sierra Peña Blanca (Chihuahua, Mexico): *Amer. Mineral.* **70,** 1290–1297.

Barron, V. and Torrent, J. (1986) Use of the Kubelka-Munk theory to study the influence of iron oxides on soil colour: *J. Soil Sci.* **37,** 499–510.

Bedidi, A. and Cervelle, B. (1993) Light scattering by spherical particles with hematite and goethite-like optical properties. Effect of water impregnation: *J. Geophys. Res.* **98,** 11,941–11,952.

Bonnin, D., Muller, S., and Calas, G. (1982) Le fer dans les kaolins. Etude par spectrométries RPE, Mössbauer, EXAFS: *Bull. Minéral.* **105,** 467–475.

Boudeulle, M. and Muller, J.-P. (1988) Structural characteristics of hematite and goethite and their relationships with kaolinite in a laterite from Cameroon. A TEM study: *Bull. Minéral.* **111,** 149–166.

Bristow, C. M. (1993) The genesis of the china clays of South-West England—A multistage story: in *Kaolin Genesis and Utilization,* H. H. Murray, W. M. Bundy, and C. C. Harvey, eds., Clay Minerals Society of America, Boulder, Colorado, 171–203.

Burns, R. G. (1985) Electronic spectra of minerals: in *Chemical Bonding and Spectroscopy in Mineral Chemistry,* F. J. Berry and D. J. Vaughan, eds., Chapman and Hall, London and New York, 63–101.

Cahill, J. E. (1979) Derivative spectroscopy: Understanding its application: *Amer. Lab.,* 79–85.

Calas, G. (1977) Les phénomènes d'altération hydrothermale et leur relation avec les minéralisations uranifères en milieu volcanique: Le cas des ignimbrites tertiaires de la Sierra de Peña Blanca, Chihuahua (Mexique): *Sci. Geol. Bull.* **30,** 3–18.

Calas, G. (1986) Spectroscopies optiques dans les minéraux: Absorption, réflectivité, luminescence: in *Méthodes Spectroscopiques Appliquées aux Minéraux* **1,** G. Calas, ed., Société française de Minéralogie et de Cristallographie, Paris, 141–185.

Combes, J.-M., Manceau, A., Calas, G., and Bottero, J.-Y. (1989) Formation of ferric oxides from aqueous solutions: A polyhedral approach by X-ray absorption spectroscopy: I. Hydrolysis and formation of ferric gels: *Geochim. Cosmochim. Acta* **53,** 583–594.

Cornell, R. M., Schneider, W., and Giovanoli, R. (1991) Preparation and characterization of colloidal α-FeOOH with a narrow range size distribution: *J. Chem. Soc. Farad. Trans.* **87,** 869–873.

Cornell, R. M. and Schwertmann, U. (1979) Influence of organic anions on the crystallization of ferrihydrite: *Clays & Clay Minerals* **27,** 402–410.

Davis, J. A. and Kent, D. B. (1990) Surface complexation modeling in aqueous geochemistry: in *Mineral-Water Interface Geochemistry, Reviews in Mineralogy, Vol. 23,* M. F. Hochella and A. F. White, eds., Mineralogical Society of America, Washington, D.C., 177–260.

Dombrowski, T. and Murray, H. H. (1984) Thorium. A key element in differentiating Cretaceous and Tertiary kaolins in Georgia and South Carolina: in *Proc. 27th Internatl. Geol. Cong., Non-Metallic Mineral Ores, Vol. 15,* VNU Science Press, Moscow, 305–317.

Dunfield, L. G. and Read, J. F. (1972) Determination of reactions rates by the use of cubic spline interpolation: *J. Chem. Phys.* **57,** 2,178–2,183.

Evans, D. L. and Adams, J. B. (1980) Amorphous gels as possible analogues to martian weathering products: *Proc. Lunar Planet. Sci. Conf.* **11,** 757–763.

Exley, C. S. and Phil, M. A. D. (1959) Magmatic differentiation and alteration in the St. Austell granite: *Q. J. Geol. Soc. London* **114,** 197–230.

Faivre, P., Herrera, V., Burgos, L., Jimenez, L., Molina, C., and Ruiz, E. (1983) Estudia general de suelos de la Comisaria de Vichada. Llanos Orientales de Colombia: *I.G.A.C.,* Bogota, 462 pp.

Herbillon, A. J., Mestdagh, M. M., Vielvoye, L., and Derouane, E. G. (1976) Iron in kaolinite with special reference to kaolinite from tropical soils: *Clay Miner.* **11,** 201–220.

Huguenin, R. L. and Jones, J. L. (1986) Intelligent information extraction from reflectance spectra: Absorption band positions: *J. Geophys. Res.* **91,** 9,585–9,598.

Hunt, G. R., Salisbury, J. W., and Lenhoff, C. J. (1971) Visible and near-infrared spectra of minerals and rocks. III. Oxides and hydroxides: *Mod. Geol.* **2,** 195–205.

Ildefonse, P., Agrinier, P., and Muller, J.-P. (1990) Crystal chemistry and isotope geochemistry of alteration associated with the uranium Nopal I deposit, Chihuahua, Mexico: *Chem. Geol.* **84,** 371–372.

Jackson, N. J., Willis-Richard, J., Manning, D. A. C., and Sams, M. S. (1989) Evolution of the Cornubian ore field, Southwest England: Part II. Mineral deposits and ore-forming processes: *Econ. Geol.* **84,** 1,101–1,133.

Jeanroy, E., Rajot, R. A., Pillon, P., and A. J. Herbillon (1991) Differential dissolution of hematite and goethite in dithionite and its implication on soil yellowing: *Geoderma* **50,** 79–94.

Jepson, W. B. (1988) Structural iron in kaolinites and in associated ancillary minerals: in *Iron in Soil and Clay Minerals,* J. W. Stucki, B. A. Goodman, and U. Schwertmann, eds., Reidel, Dordrecht, 467–536.

Jepson, W. B. and Rowse, J. B. (1975) The composition of kaolinite. An electron microscope microprobe study: *Clays & Clay Minerals* **23,** 310–317.

Kampf, N. and Schwertmann, U. (1983) Goethite and hematite in a climosequence in Southern Brazil and their

https://doi.org/10.1346/CCMN.1994.0420204 Published online by Cambridge University Press

application in classification of kaolinitic soils: *Geoderma* **29,** 27–39.

Karickhoff, S. W. and Bailey, G. W. (1973) Optical absorption spectra of clay minerals: *Clays & Clay Minerals* **21,** 59–70.

Kosmas C. S., Curi, N., Bryant, R. B., and Franzmeier, D. P. (1984) Characterization of iron oxide minerals by second derivative visible spectroscopy: *Soil Sci. Soc. Amer. J.* **48,** 401–405.

Kosmas, C. S., Franzmeier, D. P., and Schulze, D. G. (1986) Relationship among derivative spectroscopy, color, crystallite dimensions and Al-substitution of synthetic goethites and hematites: *Clays & Clay Minerals* **34,** 625–634.

Leroy, J. L., Aniel, B., and Poty, B. (1987) The Sierra Peña Blanca (Mexico) and the Meseta Los Frailes (Bolivia): The uranium concentration mechanisms in volcanic environment during hydrothermal processes: *Uranium* **3,** 211–234.

Meads, R. E. and Malden, P. J. (1975) Electron spin resonance in natural kaolinites containing Fe^{3+} and other transition metal ions: *Clay Miner.* **10,** 313–345.

Mehra, O. P. and Jackson, M. L. (1960) Iron oxide removal from soil and clays by a dithionite-citrate system buffered with sodium carbonate: *Proc. 7th Natl. Conf. Clays Clay Miner.*, Pergamon Press, New York, 317–327.

Mestdagh, M. M., Vielvoye, L., and Herbillon, A. J. (1980) Iron in kaolinite: II The relationship between kaolinite crystallinity and iron content: *Clay Miner.* **15,** 1–13.

Morris, R. V., Lauer, H. V., Lawson, C. A., Gibson, Jr., E. K., Nace, G. A., and Stewart, C. (1985) Spectral and other physicochemical properties of submicron powders of hematite (α-Fe_2O_3), maghemite (γ-Fe_2O_3), magnetite (Fe_3O_4), goethite (α-FeOOH) and lepidocrocite (γ-FeOOH): *J. Geophys. Res.* **90,** 3,126–3,144.

Morris, R. V., Neely, S. C., and Mendell, W. W. (1982) Application of Kubelka-Munk theory of diffuse reflectance to geologic problems: The role of scattering: *Geophys. Res. Lett.* **9,** 113–116.

Muller, J.-P. (1988) Analyse pétrologique d'une formation latéritique meuble du Cameroun. Essai de traçage d'une différenciation supergène par les paragenèses minérales secondaires: *Travaux et Documents Microfichés* **50,** ORSTOM, Paris, 664 pp.

Muller, J.-P. and Bocquier, G. (1986) Dissolution of kaolinites and accumulation of iron oxides in lateritic ferruginous nodules. Mineralogical and microstructural transformations: *Geoderma* **37,** 113–136.

Muller, J.-P. and Bocquier, G. (1987) Textural and mineralogical relationships between ferruginous nodules and surrounding clayey matrices in a laterite from Cameroon: in *Proc. Internatl. Clay Conf., Denver, 1985,* L. G. Schultz, H. Van Olphen, and F. A. Mumpton, eds., The Clay Minerals Society, Bloomington, Indiana, 186–196.

Muller, J.-P. and Calas, G. (1993) Genetic significance of paramagnetic centers in kaolinites: in *Kaolin Genesis and Utilization,* H. H. Murray, W. M. Bundy and C. C. Harvey, eds., Clay Minerals Society of America, Boulder, Colorado, 261–289.

Muller, J.-P., Ildefonse, P., and Calas, G. (1990) Paramagnetic defect centers in hydrothermal kaolinite from an altered tuff in the Nopal uranium deposit, Chihuahua, Mexico: *Clays & Clay Minerals* **38,** 600–608.

Murphy, P. J., Posner, A. M., and Quirk, J. P. (1976) Characterization of hydrolyzed ferric ion solutions. A comparison of the effects of various anions on the solutions: *J. Coll. Interf. Sci.* **56,** 312–319.

Murray, H. H. (1988) Kaolin minerals. Their genesis and occurrences: in *Hydrous Phyllosilicates, Reviews in Mineralogy, Vol. 19,* S. W. Bailey, ed., Mineralogical Society of America, Washington, D.C., 67–89.

O'Day, P. A., Brown, Jr., G. E., and Parks, G. A. (1990) EXAFS study of aqueous Co(II) sorption complexes on kaolinite and quartz surfaces: in *X-ray Absorption Fine Structure, Sixth Internatl. Conf. on X-ray Absorption Fine Structure, 1990, York,* S. Samar Hasnain, ed., Warrington, UK, 260–262.

Patterson, S. H. and Murray, H. H. (1984) Kaolin refractory clay, ball clay and halloysite in North America, Hawaii and the Carribean region: *Geol. Surv. Prof. Paper* **1306,** U.S. Government Printing Office, Washington, 56 pp.

Petit, S. and Decarreau, A. (1990) Hydrothermal (200°C) synthesis and crystal chemistry of iron-rich kaolinites: *Clay Miner.* **25,** 181–196.

Plançon, A., Giese, R. F., and Snyder, R. (1988) The Hinckley index for kaolinites: *Clay Miner.* **23,** 249–260.

Plançon, A., Giese, R. F., and Snyder, R., Drits, V. A., and Bookin, A. S. (1989) Stacking faults in the kaolin-group minerals: Defect structures of kaolinite: *Clays & Clay Minerals* **37,** 203–210.

Rengasamy, P. (1976) Substitution of iron and titanium in kaolinites: *Clays & Clay Minerals* **24,** 265–266.

Schwertmann, U. (1988) Occurrence and formation of iron oxides in various pedoenvironments: in *Iron in Soil and Clay Minerals,* J. W. Stucki, B. A. Goodman, and U. Schwertmann, eds., Reidel, Dordrecht, 267–308.

Schwertmann, U., and Cornell, R. M. (1991) *Iron Oxides in the Laboratory,* VCH publishers Weinheim, 101–110.

Schwertmann, U. and Murad, E. (1990) The influence of aluminum on iron oxides: XIV. Al-substituted magnetite synthesized at ambient temperatures: *Clays & Clay Minerals* **38,** 196–202.

Schwertmann, U., Murad, E., and Schulze, D. G. (1982) Is there Holocene reddening (hematite formation) in soils of axeric temperate areas?: *Geoderma* **27,** 209–223.

Schwertmann, U. and Thalmann, H. (1976) The influence of [Fe(II)], [Si] and pH on the formation of lepidocrocite and ferrihydrite during oxidation of aqueous $FeCl_2$ solutions: *Clay Miner.* **14,** 189–200.

Sheppard, S. M. F. (1977) The Cornubian batholith SW England; D/H and $^{18}O/^{16}O$ studies of kaolinite and other alteration minerals: *J. Geol. Soc. London* **133,** 573–591.

Sherman, D. M., Burns, R. G., and Burns, V. M. (1982) Spectral characteristics of the iron oxides with application to the martian bright region mineralogy: *J. Geophys. Res.* **87,** 10,169–10,180.

Sherman, D. M. and Waite, D. (1985) Electronic spectra of Fe^{3+} oxides and oxide hydroxides in the near IR to near UV: *Amer. Mineral.* **70,** 1,262–1,269.

Strens, R. G. J. and Wood, B. J. (1979) Diffuse reflectance spectra and optical properties of some iron and titanium oxides and oxyhydroxides: *Mineral. Mag.* **43,** 347–354.

Tossell, J. A., Vaughan, D. J., and Johnson, K. H. (1974) The electronic structure of rutile, wustite and hematite from molecular orbital calculations: *Amer. Mineral.* **59,** 319–334.

van Olphen, H. and Fripiat, J. J. (1978) *Data Handbook for Clay Materials and Other Non-Metallic Minerals:* Pergamon Press, Oxford, 344 pp.

Watari, F., Delavignette, P., Van Landuyt, J., and Amelinckx, S. (1983) Electron microscopic study of dehydration transformations III. High resolution observation of the reactions process FeOOH-αFe_2O_3: *J. Solid State Chem.* **48,** 49–64.

Weidner, V. R. and Hsia, J. J. (1981) Reflection properties of pressed polytetrafluoroethylene powder: *J. Opt. Soc. Amer.* **71,** 856–861.

Wendlandt, W. W. M. and Hecht, H. G. (1966) *Reflectance Spectroscopy:* Interscience publishers, John Wiley & Sons, New York, 298 pp.

(Received 19 April 1993; accepted 22 October 1993; Ms. 2364)

https://doi.org/10.1346/CCMN.1994.0420204 Published online by Cambridge University Press